Electronic Supplementary Material (ESI) for Journal of Materials Chemistry C.

Supporting Information

Efficient *M*-shaped blue emitters having high conjugation extent with improved roll-off efficiency

Jayaraman Jayabharathi*, Venugopal Thanikachalam, Shanmugam Thilagavathy, Jagathratchagan Anudeebhana

Department of Chemistry, Annamalai University, Annamalai nagar, Tamilnadu- 608 002, India.

Address for correspondence

*Dr. J. Jayabharathi
Professor of Chemistry
Department of Chemistry
Materials science lab
Annamalai University
Annamalai nagar 608 002
Tamilnadu, India.
E-mail: jtchalam2005@yahoo.co.in

Contents

Scheme 1. Schematic representation of blue emitters.

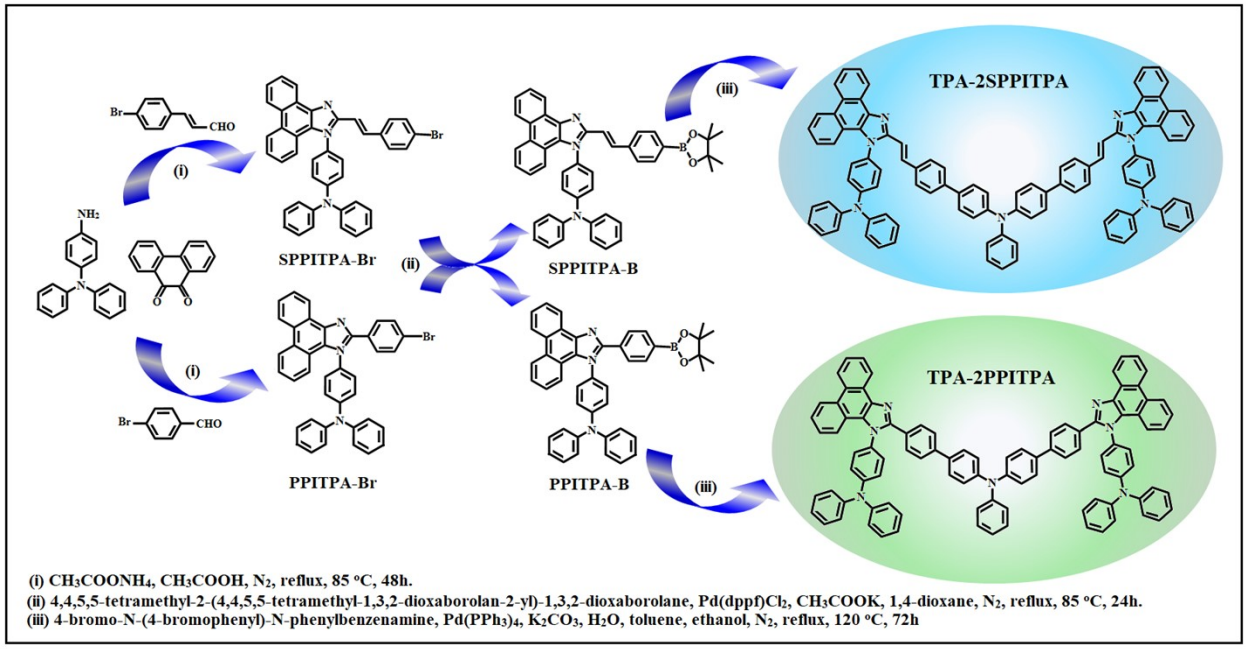

SI-II. Experimental Section

The chemicals used in the experimental section were obtained from Sigma-Aldrich. Synthetic route of the multifunctional materials were outlined in Scheme S1.

(i)N-(4-(2-(4-bromophenyl)-1H-phenanthro[9,10-d]imidazol-1-yl)phenyl)-N-phenylbenzenamine (PPITPA-Br)

A mixture of 9,10-phenanthrenequinone (2.54 mmol), 4-bromobenzaldehyde (3.06 mmol), ammonium acetate (25.4 mmol) and N^1, N^1-diphenylbenzene-1,4-diamine (2.02 mmol) in acetic acid (10 mL) was refluxed with stirring for 48 h (85°C; N_2**)**. The crude was purified by column chromatography. Yield: 72%. ^{1}H NMR (400 MHz, $CDCl_3$, δ, ppm): 6.22 (d, 6H), 6.42 (m, 2H), 6.82-7.16 (m, 6H), 7.46-7.62 (m, 8H), 7.83-8.08 (m, 4H). ^{13}C NMR (100 MHz, $CDCl_3$, δ, ppm): 112.7, 118.3, 120.6, 124.8, 126.0, 129.0, 132.6, 138.3, 140.8, 145.3. MS: m/z. 616.55 [M^+]; Calcd. 616.40.

(ii)N-(4-(2-(4-bromostyryl)-1H-phenanthro[9,10-d]imidazol-1-yl)phenyl)-N-phenylbenzenamine (SPPITPA-Br)

A mixture of 9,10-phenanthrenequinone (2.54 mmol), 4-bromocinnamaldehyde (3.06 mmol), ammonium acetate (25.4 mmol) and N^1, N^1-diphenylbenzene-1,4-diamine (2.02 mmol) in acetic acid (10 ml) was refluxed with stirring for 48 h (85°C; N_2**)**. The crude was purified by column chromatography. Yield: 74%. ^{1}H NMR (400 MHz, $CDCl_3$, δ, ppm): 6.08 (d, 6H), 7.91-8.00 (m, 6H), 6.80 (s, 1H), 7.18 (s, 1H) ,7.25-7.41 (m, 8H), 7.63-7.80 (m, 6H), 7.91-8.00 (m, 6H). ^{13}C NMR (100 MHz, $CDCl_3$, δ, ppm): 110.0, 121.3, 123.0, 125.6, 127.1, 128.0, 131.3, 133.0, 135.5, 140.5, 143.4. MS: m/z. 642.59 [M^+]; Calcd. 642.51.

(iii) N-(4-(2-(4-(4,4,5,5-tetramethyl-1,3,2-dioxaborolan-2-yl)phenyl)-1H-phenanthro[9,10-d]imidazol-1-yl)phenyl)-N-phenylbenzenamine (PPITPA-B)

A mixture of PPITPA-Br (5.56 mmol), 4,4,5,5-tetramethyl-2-(4,4,5,5-tetramethyl-1,3,2-dioxaborolan-2-yl)-1,3,2-dioxaborolane (7.61 mmol), $PdCl_2$(dppf) (0.11 mmol), CH_3COOK

(33.36 mmol) and 1, 4-dioxane was degassed, stirred and refluxed (85 °C; 24 h; N_2 stream). The reaction mixture was washed with distilled water and then extracted with tetrahydrofuran. The crude was purified by silica gel chromatography to afford white solid. Yield: 71%. ^{1}H NMR (400 MHz, $CDCl_3$, δ, ppm): 1.20 (s, 12H), 6.61-6.80 (m, 6H), 6.91-7.29 (m, 6H), 7.42-7.68 (m, 6H), 7.82-8.01 (m, 8H). ^{13}C NMR (100 MHz, $CDCl_3$, δ, ppm): 20.6, 80.1, 123.0, 125.0, 126.8, 127.8, 131.0, 135.8, 145.9. MS: m/z. 663.61 [M^+]; Calcd. 663.26.

(iv)(E)-N,N-diphenyl-4-(2-(4-(4,4,5,5-tetramethyl-1,3,2-dioxaborolan-2-yl)styryl)-1H-phenanthro[9,10-d]imidazol-1-yl)aniline (SPPITPA-B)

A mixture of SPPITPA-Br (5.56 mmol), 4,4,5,5-tetramethyl-2-(4,4,5,5-tetramethyl-1,3,2-dioxaborolan-2-yl)-1,3,2-dioxaborolane (7.61 mmol), $PdCl_2$(dppf) (0.11 mmol), CH_3COOK (33.36 mmol) and 1, 4-dioxane was degassed, stirred and refluxed (85 °C; 24 h; N_2 stream). The reaction mixture was washed with distilled water and then extracted with tetrahydrofuran and the crude was purified by silica gel chromatography to afford white solid. Yield: 73%. ^{1}H NMR (400 MHz, $CDCl_3$, δ, ppm): 1.18 (s, 12H), 6.82 (s, 1H), 7.16 (s, 1H), 6.76-6.86 (m, 6H), 7.28-7.40 (m, 6H), 7.72-8.10 (m, 8H). ^{13}C NMR (100 MHz, $CDCl_3$, δ, ppm): 20.0, 117.0, 122.1, 125.0, 126.8, 127.0, 133.9, 136.5, 141.0, 145.7. MS: m/z. 689.65 [M^+]; Calcd. 689.61.

(v)4'-(1-(4-(diphenylamino)phenyl)-1H-phenanthro[9,10-d]imidazol-2-yl)-N-(4'-(1-(4-(diphenylamino)phenyl)-1H-phenanthro[9,10-d]imidazol-2-yl)-[1,1'-biphenyl]-4-yl)-N-phenyl-[1,1'-biphenyl]-4-amine (TPA-2PPITPA)

A mixture of PPITPA-B (4.50 mmol), 4-bromo-N-(4-bromophenyl)-N-phenylbenzenamine (2.00 mmol), potassium carbonate (42 mmol), toluene (21 ml): ethanol (10.5 ml) and deionized water (14 ml) with $Pd(PPh_3)_4$ (0.08 mmol) was refluxed (120 ^{o}C; 72 h; N_2 stream). The mixture was cooled and water was added and extracted with THF. The crude was purified by chromatography to afford pale yellow solid. Yield: 76%. ^{1}H NMR (400 MHz, $CDCl_3$, δ, ppm): 6.46-6.70 (m, 12H), 6.82-6.90 (m, 8H), 7.15-7.36 (m, 8H), 7.43-7.56 (m, 12H), 7.68-8.00 (m, 14H),

8.10-8.68 (m, 11H). ^{13}C NMR (100 MHz, $CDCl_3$, δ, ppm): 110.0, 120.4, 123.8, 125.8, 126.0, 126.9, 127.8, 128.0, 129.4, 132.0, 133.3, 138.0, 141.3, 145.0. MS: m/z. 1316.59 [M^+]; Calcd. 1316.36. Anal. Cacld (%) for $C_{96}H_{65}N_7$: C, 87.58; H, 4.98; N, 7.45. Found: C, 87.54; H, 4.95; N, 7.41.

(vi)4'-((E)-2-(1-(4-(diphenylamino)phenyl)-1H-phenanthro[9,10-d]imidazol-2-yl)vinyl)-N-(4'-((E)-2-(1-(4-(diphenylamino)phenyl)-1H-phenanthro[9,10-d]imidazol-2-yl)vinyl)-[1,1'-biphenyl]-4-yl)-N-phenyl-[1,1'-biphenyl]-4-amine (TPA-2SPPITPA)

A mixture of SPPITPA-B (4.50 mmol), 4-bromo-N-(4-bromophenyl)-N-phenylbenzenamine (2.00 mmol), potassium carbonate (5.80 g, 42 mmol), toluene (21 ml): ethanol (10.5 ml) and deionized water (14 ml), with $Pd(PPh_3)_4$ (0.08 mmol) was refluxed (120 ^oC; 72 h; N_2 stream). The mixture was cooled down and extracted with THF. The crude was purified by chromatography to afford yellow solid. Yield: 75%. ^{1}H NMR (400 MHz, $CDCl_3$, δ, ppm): 6.30 (m, 6H), 6.32-6.42 (m, 6H), 6.62-6.79 (s, 9H), 6.96-7.18 (m, 16H), 7.28-7.40 (m, 7H), 7.42-7.56 (m, 7H), 7.68-7.72 (s, 8H), 8.08-8.19 (m, 10H).^{13}C NMR (100 MHz, $CDCl_3$, δ, ppm): 117.0, 122.8, 123.8, 125.0, 126.8, 127.0, 128.8, 129.0, 132.4, 137.6, 140.0, 144.8. MS: m/z. 1368.66 [M^+]; Calcd. 1368.49. Anal. Cacld (%) for $C_{100}H_{69}N_7$: C, 87.75; H, 5.08; N, 7.16. Found: C, 87.73; H, 5.04; N, 7.13.

SI-III. (i) General information

All the reagents and solvents were purchased from commercial sources and used as received. The emitters were subjected to sublimation to enhance the purity before photoluminescence and electroluminescence investigations. ^{1}H and ^{13}C NMR spectra were recorded at room temperature on Bruker 400 spectrometer in CD_2Cl_2. The mass spectra were recorded on Agilent LCMS VL SD. The UV-Vis spectra were recorded on Lambda 35 PerkinElmer (solution)/ Lambda 35 spectrophotometer (RSA-PE-20) (film). The emission spectra were recorded with Perkin Elmer LS55 spectrometer and quantum yield was measured with

fluorescence spectrometer (Model-F7100 with integrating sphere). The decomposition temperature (T_d) and glass transition temperature (T_g) were measured with NETZSCH (DSC-204) (10° C min^{-1}; N_2 atmosphere), respectively. Fluorescence lifetime was estimated by time correlated single-photon counting (TCSPC) method on Horiba Fluorocube-01-NL lifetime system: nano LED is an excitation source with TBX-PS is detector; DAS6 software was employed to analyse the decay by reconvolution method. The low temperature optical measurement and absolute quantum yield (PLQY) was determined with fluorescence spectrometer Model-F7100. The quantum yield (ϕ) was measured in dichloromethane with 0.5 M H_2SO_4 solution of quinine (0.54) as reference and calculated using the equation: $\phi_{unk} = \phi_{std}\left(\frac{I_{unk}}{I_{std}}\right)\left(\frac{A_{std}}{A_{unk}}\right)\left(\frac{\eta_{unk}}{\eta_{std}}\right)^2$, where ϕ_{unk} and ϕ_{std} are the quantum yield of the sample and standard respectively. I_{unk} and I_{std} are the integrated emission intensities of the sample and standard, respectively. η_{unk} and η_{std} are the refractive indices of the sample and standard solution and A_{unk} and A_{std} are the absorbance of these sample and standard, respectively. The quantum yield of thin materials in film has been measured on quartz plate using an integrating sphere [1]. Oxidation potentials were measured from potentiostat electrochemical analyzer (CHI 630A) in dichloromethane at a scan rate of 100 mV s^{-1}, platinum wire as auxiliary electrode, glass carbon disk as working electrode and Ag/Ag^+ as reference electrode. Ferrocene was used as an internal standard with HOMO of -4.80 eV and 0.1M tetrabutylammoniumperchlorate in CH_2Cl_2 as supporting electrolyte. All density functional theory (DFT) calculations were carried out using Gaussian 09 package [2] and Multiwfn [2]. The ground-state (S_0) geometries in the gas phase were initially optimized at the level of B3LYP/6-31G (d, p), a commonly used level for the precise geometry optimization. Then, geometry optimization and excited-state properties based on S_1 geometries were studied using time-dependent DFT (TD-DFT)

at the same level. The natural transition orbitals (HONTOs and LUNTOs) with hole-particle contribution, transition density matrix and overlap integral have been studied in detail [3-5].

(ii) OLEDs fabrication and measurement

ITO glass (resistance 20 Ω/sq) were cleaned with acetone, deionized water and isopropanol and dried (120 ^{o}C) followed by UV-zone treatment (20 min) and transferred into deposition system. The devices were fabricated by multiple source beam deposition method (vacuum pressure - 4 × 10^{-5} mbar). Evaporation rate of 2-4 Å s^{-1} (organic materials) and 0.1 and 4 Ås^{-1} for LiF and metal electrodes were applied, respectively. The thickness of each decomposition layer was monitored with quartz crystal thickness monitor. The EL measurement was recorded with USB-650-VIS-NIR spectrometer (Ocean Optics, Inc, USA). The current density-voltage-luminance (J-V-L) characteristics were performed using source meter (Keithley 2450) equipped with LS-110 light intensity meter. The external quantum efficiency was determined from luminance, current density and EL spectrum assuming Lambertian distribution.

SI–IV. Charge-Transfer indexes

The hole-particle pair interactions have been related to the distance covered during the excitations, one possible descriptor Δr index could be used to calculate the average distance which is weighted in function of the excitation coefficients.

$$\Delta r = \frac{\Sigma_{ia} k_{ia}^2 \left| \langle \varphi_a | r | \varphi_a \rangle - \langle \varphi_i | r | \varphi_i \rangle \right|}{\Sigma_{ia} K_{ia}^2} \quad \text{…….. (S1)}$$

where $\left| \langle \varphi_i | r | \varphi_i \rangle \right|$ is the norm of the orbital centroid [6-9]. Δr-index will be expressed in Å.

The density variation associated to the electronic transition is given by

$$\Delta\rho(r) = \rho_{EX}(r) - \rho_{GS}(r) \quad \text{..... (S2)}$$

where $\rho_{GS}(r)$ and $\rho_{EX}(r)$ are the electronic densities of to the ground and excited states, respectively. Two functions, $\rho_+(r)$ and $\rho_-(r)$, corresponds to the points in space where an increment or a depletion of the density upon absorption is produced and they can be defined as follows:

$$\rho_+(r) = \begin{Bmatrix} \Delta\rho(r) & if\ \Delta\rho(r) > 0 \\ 0 & if\ \Delta\rho(r) < 0 \end{Bmatrix} \quad \text{..... (S3)}$$

$$\rho_-(r) = \begin{Bmatrix} \Delta\rho(r) & if\ \Delta\rho(r) < 0 \\ 0 & if\ \Delta\rho(r) > 0 \end{Bmatrix} \quad \text{..... (S4)}$$

The barycenters of the spatial regions R_+ and R_- are related with $\rho_+(r)$ and $\rho_-(r)$ and are shown as

$$R_+ = \frac{\int r\rho_+(r)dr}{\int \rho_+(r)dr} = (x_+, y_+, z_+) \quad \text{..... (S5)}$$

$$R_- = \frac{\int r\rho_-(r)dr}{\int \rho_-(r)dr} = (x_-, y_-, z_-) \quad \text{..... (S6)}$$

The spatial distance (D_{CT}) between the two barycenters R_+ and R_- of density distributions can thus be used to measure the CT excitation length

$$D_{CT} = |R_+ - R_-| \quad \text{..... (S7)}$$

The transferred charge (q_{CT}) can be obtained by integrating over all space $\rho_+(\rho_-)$,. Variation in dipole moment between the ground and the excited states (μ_{CT}) can be computed by the following relation:

$$\|\mu_{CT}\| = D_{CT}\int \rho_+(r)dr = D_{CT}\int \rho_-(r)dr \quad \text{..... (S8)}$$

$$= D_{CT} q_{CT} \quad \text{..... (S9)}$$

The difference between the dipole moments $\|\mu_{CT}\|$ have been computed for the ground and the excited states $\Delta\mu_{ES-GS}$. The two centroids of charges (C^+/C^-) associated to the positive and negative density regions are calculated as follows. First the root–mean–square deviations along the three axis (σ_{aj}, j = x, y, z; a = + or –) are computed as

$$\sigma_{a,j} = \sqrt{\frac{\sum_i \rho_a(r_i)(j_i - j_a)^2}{\sum_i \rho_a(r_i)}} \quad \text{..... (S10)}$$

The two centroids (C_+ and C_-) are defined as

$$C_+(r) = A_+ \, e\left(-\frac{(x-x_+)^2}{2\sigma_{+x}^2} - \frac{(y-y_+)^2}{2\sigma_{+y}^2} - \frac{(z-z_+)^2}{2\sigma_{+z}^2}\right) \quad \text{..... (S11)}$$

$$C_{-+}(r) = A_- \, e\left(-\frac{(x-x_-)^2}{2\sigma_{-x}^2} - \frac{(y-y_-)^2}{2\sigma_{-y}^2} - \frac{(z-z_-)^2}{2\sigma_{-z}^2}\right) \quad \text{..... (S12)}$$

The normalization factors (A+ and A_) are used to impose the integrated charge on the centroid to be equal to the corresponding density change integrated in the whole space:

$$A_+ = \frac{\int \rho_+(r)dr}{\int e(-\frac{(x-x_-)^2}{2\sigma_{+x}^2} - \frac{(y-y_-)^2}{2\sigma_{+y}^2} - \frac{(z-z_-)^2}{2\sigma_{+z}^2})dr} \quad \text{..... (S13)}$$

$$A_- = \frac{\int \rho_-(r)dr}{\int e(-\frac{(x-x_-)^2}{2\sigma_{-x}^2} - \frac{(y-y_-)^2}{2\sigma_{-y}^2} - \frac{(z-z_-)^2}{2\sigma_{-z}^2})dr} \quad \text{..... (S14)}$$

H index is defined as half of the sum of the centroids axis along the D–A direction, if the D–A direction is along the X axis, H is defined by the relation:

$$H = \frac{\sigma_{+x} + \sigma_{-x}}{2} \quad \text{..... (S15)}$$

The centroid along X axis is expected. The t index represents the difference between D_{CT} and H:

$$t = D_{CT} - H \quad \text{..... (S16)}$$

SI-V. Figures

Figure S1. Natural transition orbital pairs (HONTOs and LUNTOs) with transition character for singlet states of TPA-2PPITPA [*f*-oscillator strength and % weights of hole-particle].

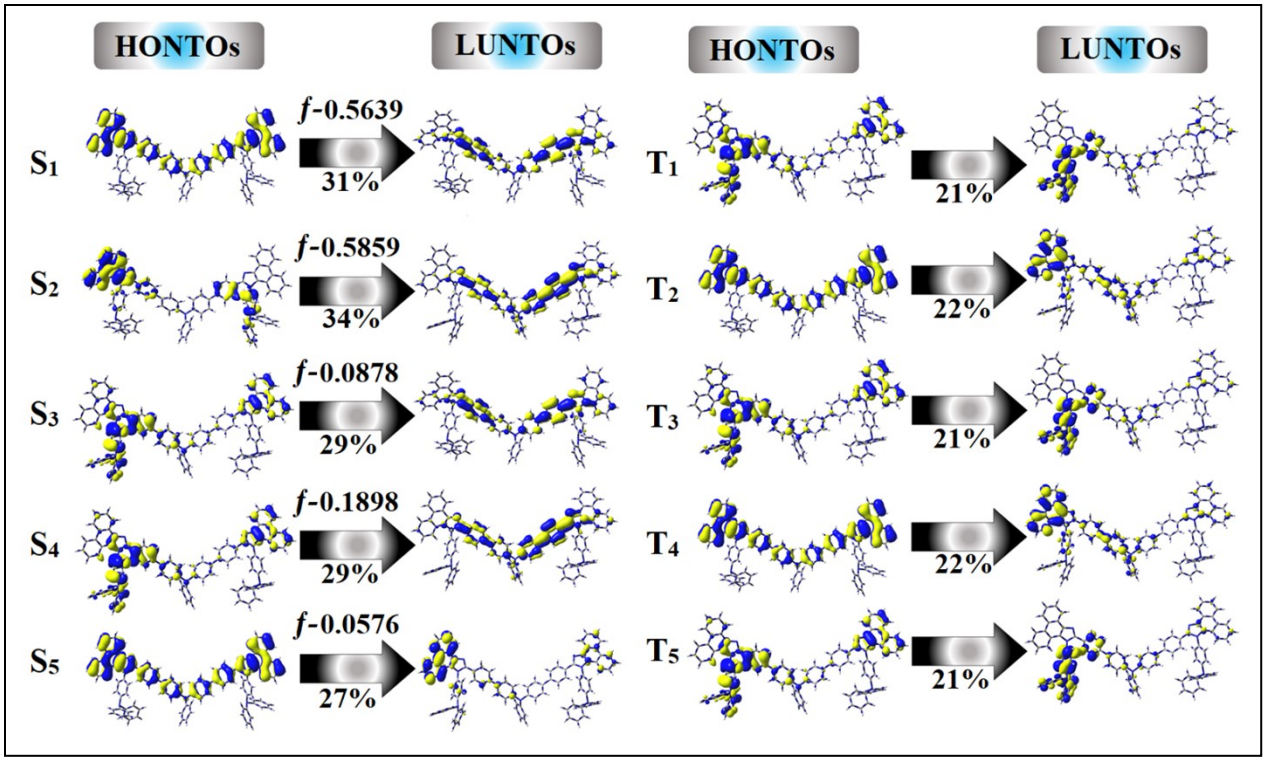

SI-VI. (a) Solvatochromism for HLCT character

The optical characteristics of emissive materials were studied in solution by absorption and emission studies. The emission peak was red shifted as increasing the solvent polarity because of

polarization induced optical shift (Tables S3 and S4: Figure S2). The PL spectra gradually widened indicates that their excited state possess strong CT character when compared to ground state and further stabilized by polar solvents.

Figure S2. (a) Solvatochromic absorption and (b) emission spectra of TPA-2PPITPA and TPA-2SPPITPA.

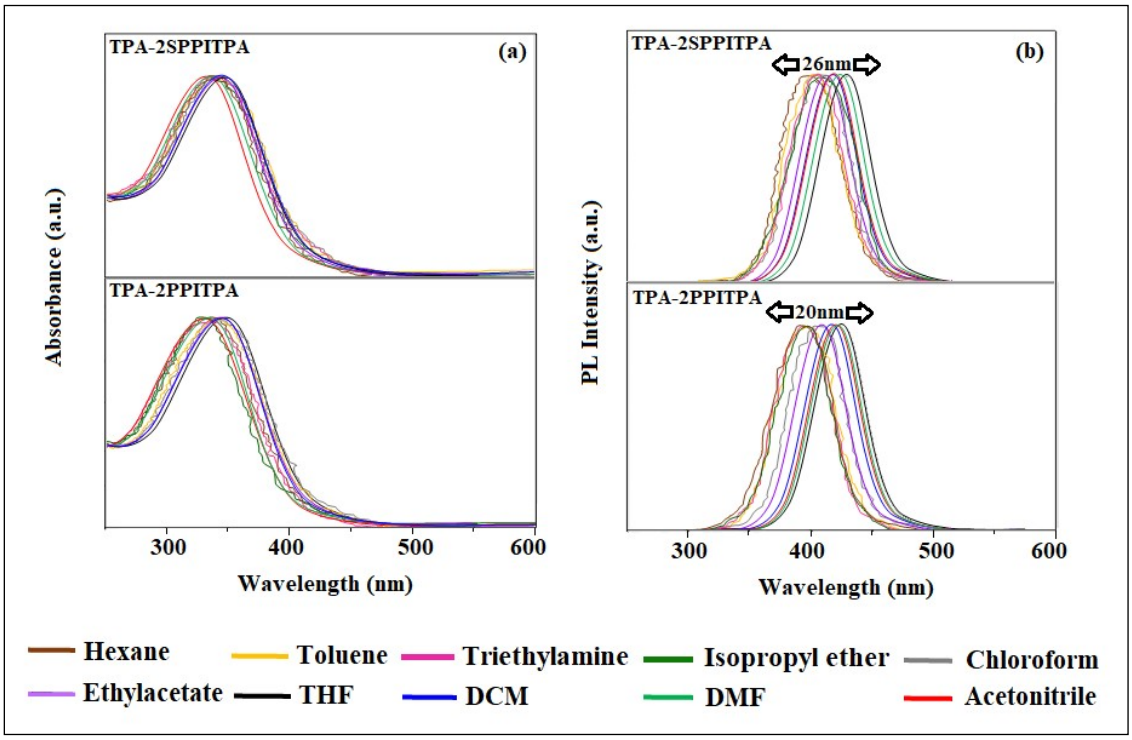

Figure S3. (a) Non-equivalent hybridization, (b) Schematic representation of RISC process of TPA-2PPITPA, (c) Transient EL decay of TPA-2SPPITPA at different voltages and (d) Amplified EL decay of the delayed component of TPA-2SPPITPA.

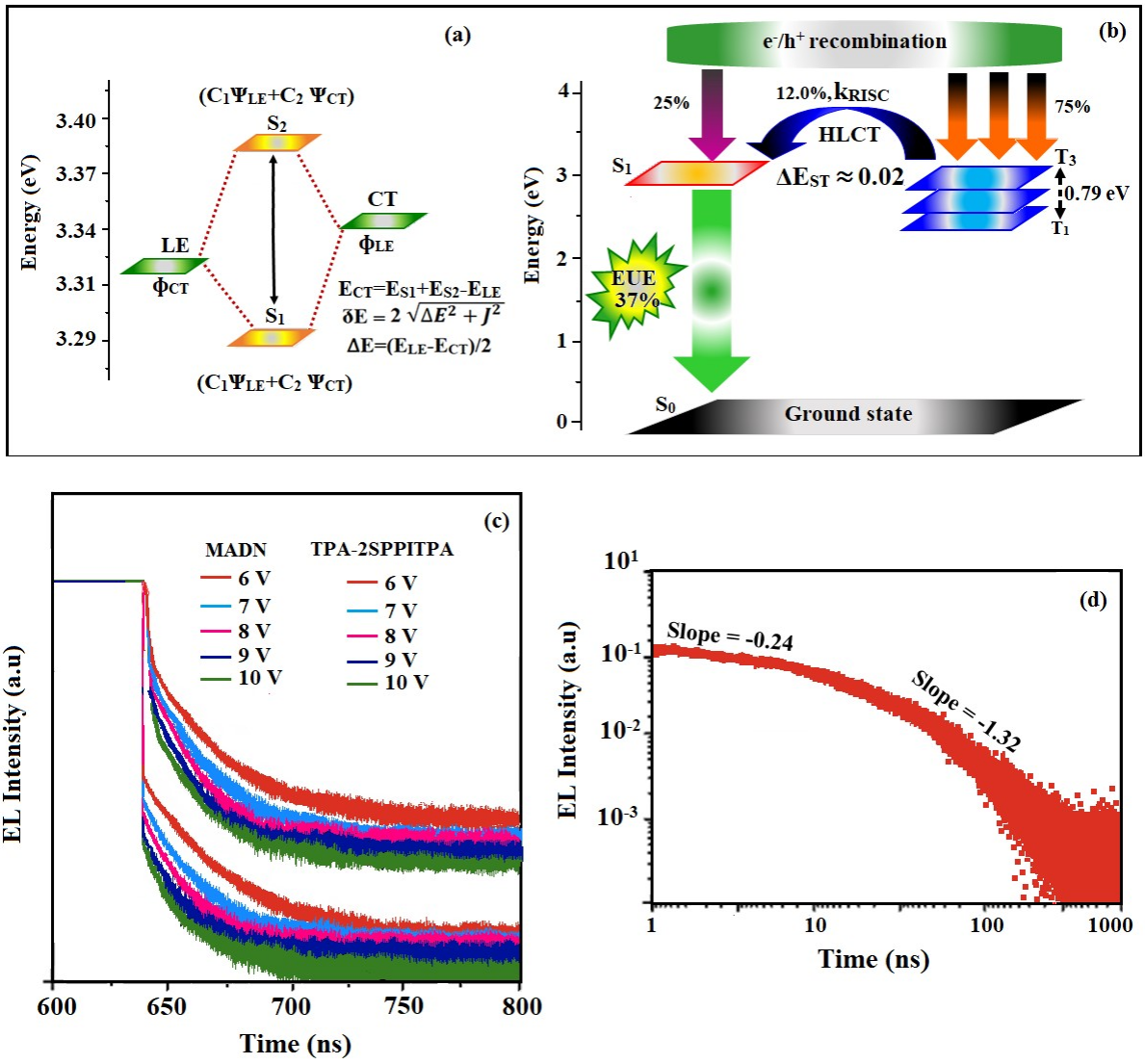

(b) Transition density matrix (TDM) and hole-particle distribution

Transition density matrix (TDM) and electron-hole pair studies have been employed as a tool to explore LE and CT components in HLCT of TPA-2PPITPA and TPA-2SPPITPA (Figure S4 and Figure S5: Tables S5-S8). The diagonal and off-diagonal part of TDM plot confirm LE and CT components, respectively. On excitation of TPA-2PPITPA and TPA-2SPPITPA, the

transferred electron delocalized from donor to acceptor which is confirmed by electron density contribution in both ground and excited states of TPA-2PPITPA and TPA-2SPPITPA. The hole and electron density in TPA-2PPITPA and TPA-2SPPITPA have been depicted in Tables S5-S8. The *H*/*t* indexes of TPA-2PPITPA and TPA-2SPPITPA have been calculated as 9.24/8.71 and 11.77/9.61 with overlap integral (C^+/C^-) of 0.99 and 0.93, respectively (Table S9). The D_{CT} of *m*-TPA-2PPITPA and TPA-2SPPITPA was found to be 0.53 and 2.33, respectively (Figure S6). The non-zero *t* index implies the effective overlap of hole and electron in all directions. The Δr index (equation S1: h^+- e^- distance: $d_{h^+-e^-}$) inferred the type of excitation, short and larger distances ($d_{h^+-e^-}$) correspond to LE and CT excitation, respectively.

Figure S4. Hole and particle electron density distribution [green increasing and blue decreasing electron density] and Transition density matrix (TDM) plot of TPA-2SPPITPA.

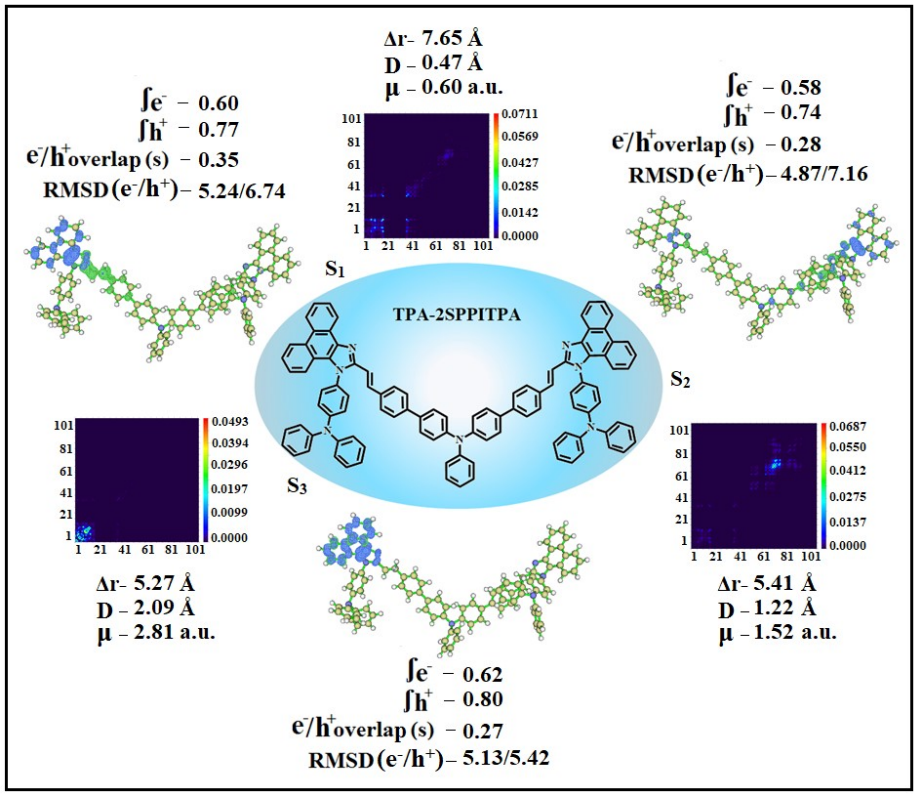

Figure S5. Hole and particle electron density distribution [green increasing and blue decreasing electron density] and Transition density matrix (TDM) plot of TPA-2PPITPA.

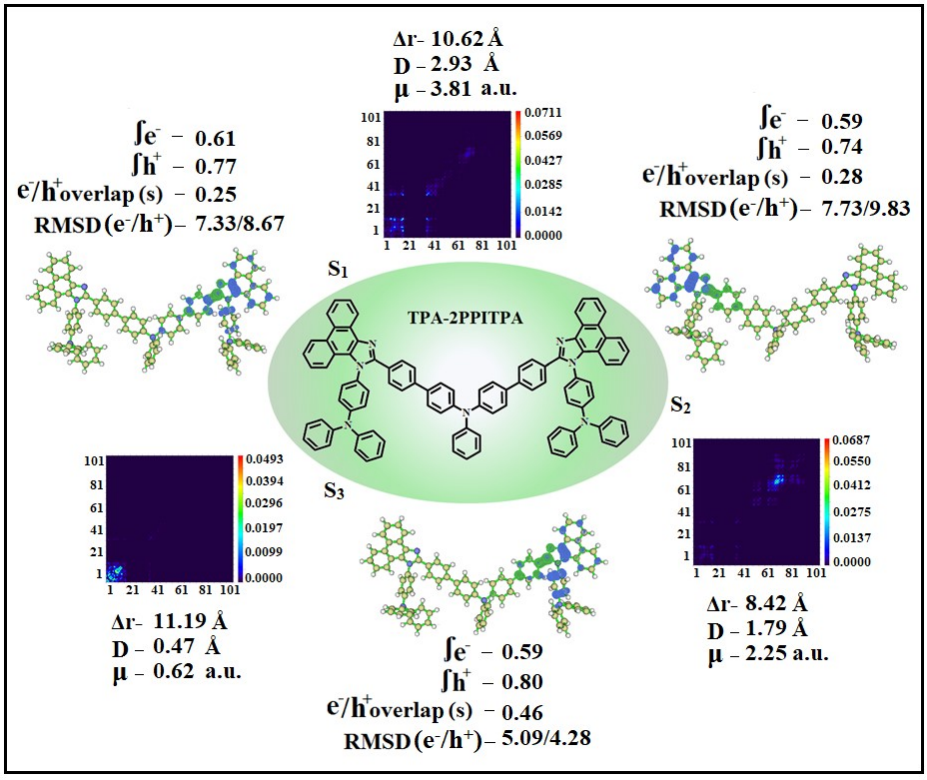

Figure S6. Graphical representation of D_{CT} and centroid of charges [C+(r) / C-(r); isosurface (0.1 a.u)].

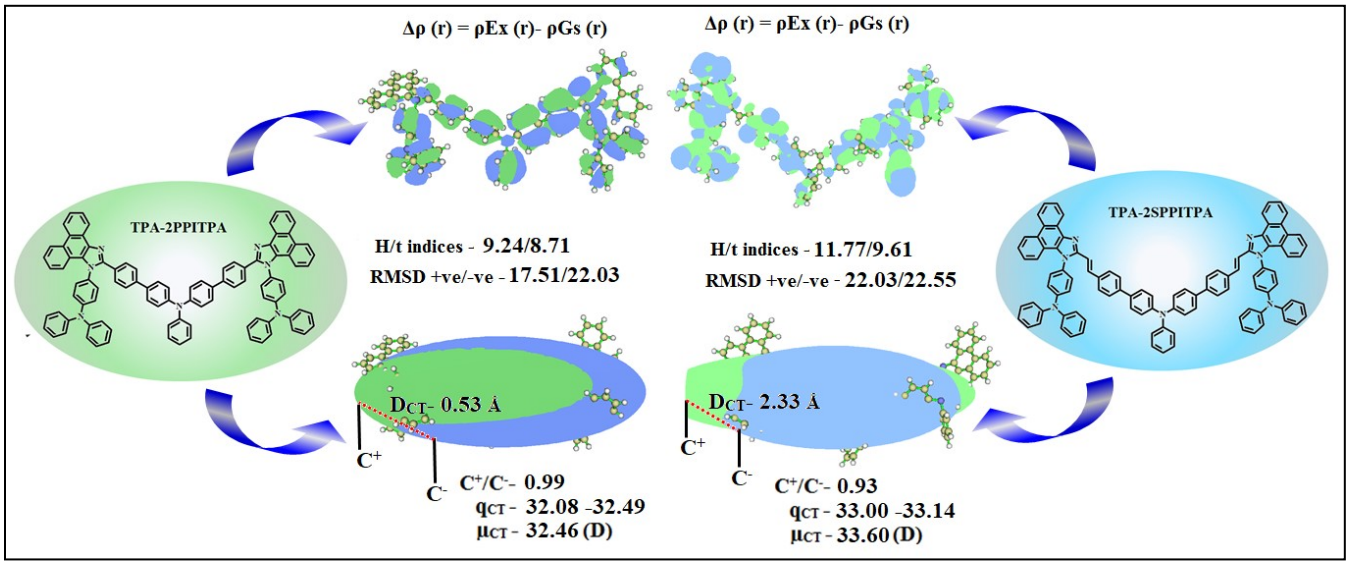

(c) Potential energy scan (PES)

The potential energy surface (PES) scan have been plotted as a function of twist angle between C2 substituent and phenanthroimidazole core in gas phase and different polar solvents (Figures S7). In gas phase, it is impossible for S3 mixing with S1 state as a result of large energy gap between them. An increasing solvent polarity, the large dipole moment of S3 state leads to energetic stabilization. In low polarity solvent (hexane), S3 state can intercross with S1 state whereas in high polarity solvent (acetonitrile), S3 state energy decreases sharply and becomes lowest excited state. In moderate polar solvents (chloroform), the energetic closeness results in an enhanced mixing of S3 with S1. Therefore, S1 state is dominated by LE character in low polar medium; S1 state is dominated by mixing LE and CT character in moderate polar medium and S1 state is dominated by CT character in high polar medium.

Figure S7. Potential energy surface scan (PES) diagram of (a) TPA-2SPPITPA and (b) TPA-2PPITPA.

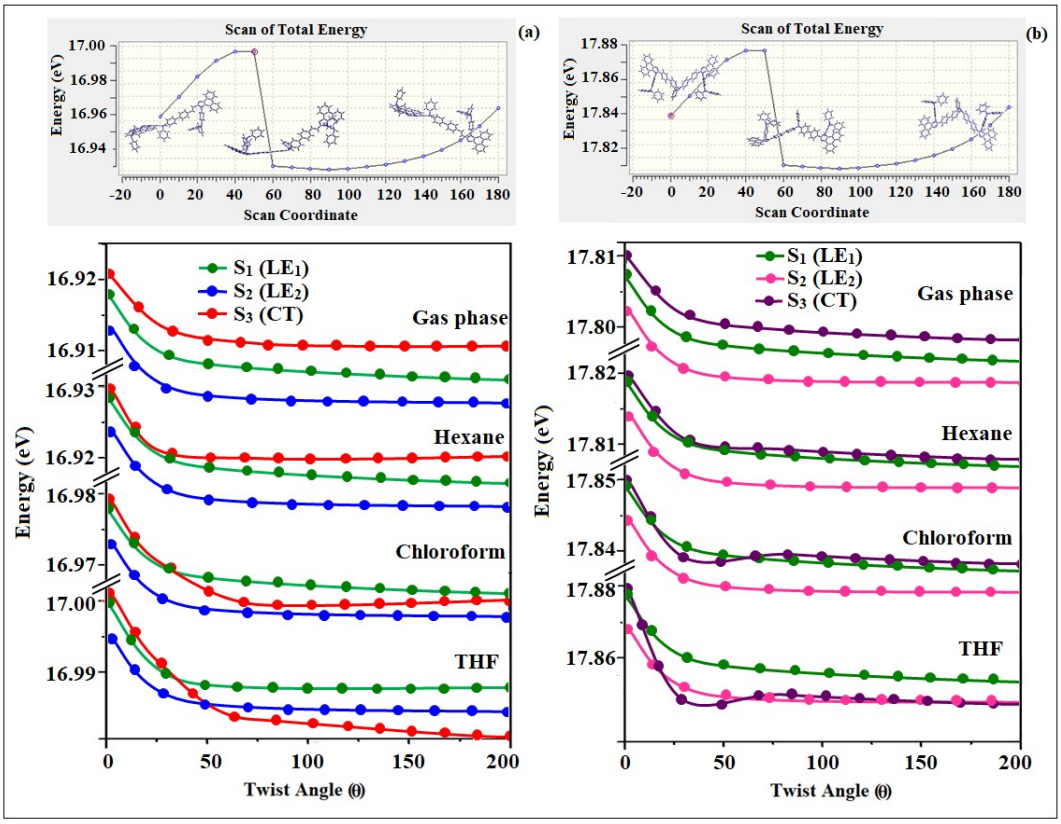

SI-VII: Tables

Table S1. Computed [zindo (Singlet or Triplet, n states=10)] singlet (E_S) and triplet (E_T) energies (eV), oscillator strength (*f*) and Δr index (Å) of TPA-2PPITPA from NTOs.

Energy level	E_S	Oscillator strength (*f*)	Δr index	NTO Transitions	E_T	Δr index	NTO Transitions
1	3.29	0.5639	7.65	$242 \xrightarrow{31\%} 244$	2.48	3.62	$241 \xrightarrow{21\%} 246$
2	3.39	0.5859	5.41	$240 \xrightarrow{34\%} 243$	2.83	6.40	$242 \xrightarrow{22\%} 245$
3	3.42	0.0878	5.27	$241 \xrightarrow{29\%} 244$	3.27	3.48	$241 \xrightarrow{21\%} 246$
4	3.51	0.1898	3.93	$241 \xrightarrow{29\%} 244$	3.66	5.08	$242 \xrightarrow{22\%} 245$
5	3.54	0.0576	5.94	$242 \xrightarrow{27\%} 248$	3.98	3.12	$241 \xrightarrow{21\%} 246$

Table S2. Computed [zindo (Singlet or Triplet, n states=10)] singlet (E_S) and triplet (E_T) energies (eV), oscillator strength (*f*) and Δr index (Å) of TPA-2SPPITPA from NTOs.

Energy level	E_S	Oscillator strength (f)	Δr index	NTO Transitions	E_T	Δr index	NTO Transitions
1	3.32	1.2234	10.62	36% 252 → 253	2.50	6.47	22% 251 → 254
2	3.37	0.5532	8.42	35% 251 → 254	2.96	10.13	22% 251 → 254
3	3.62	0.0326	11.19	21% 252 → 258	3.32	7.91	22% 251 → 254
4	3.64	0.0441	9.56	42% 250 → 254	1.71	7.98	22% 251 → 254
5	3.73	0.3825	7.14	20% 251 → 253	1.73	9.05	22% 251 → 254

Table S3. Photophysical properties of TPA-2PPITPA in different solvents.

Solvents	**ε**	**n**	***f*** **(ε, n)**	**λ_{ab} (nm)**	**υ_{ab} (cm^{-1})**	**λ_{flu} (nm)**	**υ_{flu} (cm^{-1})**	**υ_{ss} (cm^{-1})**
Hexane	1.88	1.37	0.00041	343	29154	402	24876	4279
Toluene	2.38	1.49	0.014	344	29070	406	24631	4440
Triethylamine	2.42	1.40	0.048	341	29326	404	24752	4573
Isopropyl ether	3.88	1.36	0.145	341	29325	405	24691	4634
Chloroform	4.81	1.45	0.148	346	28901	414	24155	4747
ethyl acetate	6.09	1.41	0.186	347	28818	419	23866	4952
THF	7.52	1.41	0.209	351	28490	430	23256	5234
dichloromethane	9.08	1.42	0.218	346	28902	425	23529	5372
DMF	36.7	1.43	0.276	343	29155	428	23364	5790
acetonitrile	37.5	1.34	0.305	338	29586	427	23419	6167

Table S4. Photophysical properties of TPA-2SPPITPA in different solvents.

Solvents	**ε**	**n**	***f*** **(ε, n)**	**λ_{ab} (nm)**	**υ_{ab} (cm^{-1})**	**λ_{flu} (nm)**	**υ_{flu} (cm^{-1})**	**υ_{ss} (cm^{-1})**
Hexane	1.88	1.37	0.00041	335	29851	396	25253	4598
Toluene	2.38	1.49	0.014	336	29762	400	25000	4762
Triethylamine	2.42	1.40	0.048	336	29761	401	24938	4824
Isopropyl ether	3.88	1.36	0.145	335	29851	403	24814	5037
Chloroform	4.81	1.45	0.148	337	29674	408	24510	5164
ethyl acetate	6.09	1.41	0.186	338	29586	412	24272	5314
THF	7.52	1.41	0.209	342	29240	422	23697	5543
dichloromethane	9.08	1.42	0.218	340	29412	420	23810	5602
DMF	36.7	1.43	0.276	334	29940	421	23753	6187
acetonitrile	37.5	1.34	0.305	331	30211	420	23810	6402

Table S5. Computed hole and electron overlap (S), distance between centroids of hole and electron (D, Å) and dipole moment (μ) for singlet states of TPA-2PPITPA.

State	Hole integral	Electron integral	Integral of transition density	Integral overlap of h^+- e^- (S)	Centroid of hole (Å)			Centroid of electron (Å)			D (Å)	μ (a.u)
					x	y	z	x	y	z		
S1	0.7671	0.5990	-0.0038	0.3515	7.5329	2.0478	0.1993	7.0707	2.1139	0.2128	0.46	0.60
S2	0.7438	0.5772	-0.0095	0.2791	-8.8061	3.2611	-0.0329	-8.0048	2.4101	-0.3704	1.21	1.51
S3	0.8014	0.6166	-0.0085	0.2655	9.2841	1.7061	0.2508	7.2447	2.1812	0.1903	2.09	2.80
S4	0.6347	0.4591	0.0015	0.2436	7.8699	-0.0406	0.2363	7.6782	-0.0080	0.2106	0.19	0.20
S5	0.7753	0.5727	-0.0057	0.4281	10.5494	4.0911	0.1956	11.0562	3.8357	0.2326	0.56	0.72
T1	0.5415	0.3792	0.0072	0.2997	7.5459	-0.1168	0.2714	8.0048	-0.4083	0.1462	0.55	0.48
T2	0.6521	0.4827	0.0070	0.4192	10.0178	3.8792	0.2207	10.0514	3.5581	0.2554	0.32	0.34
T3	0.4337	0.3022	-0.0000	0.2330	-7.7864	0.3493	-0.4690	-7.9820	0.4405	-0.5013	0.21	0.15
T4	0.4010	0.2936	0.0080	0.2054	-8.5306	2.2893	-0.1239	-7.0749	1.7284	-0.3054	1.57	1.03
T5	0.3128	0.2295	0.0078	0.1635	2.4785	0.0595	-0.0402	3.6573	0.9669	-0.0988	1.48	0.76

Table S6. Computed hole and electron overlap (S), distance between centroids of hole and electron (D, Å) and dipole moment (μ) for singlet states of TPA-2SPPITPA.

State	Hole integral	Electron integral	Integral of transition density	Integral overlap of h^+- e^- (S)	Centroid of hole (Å)			Centroid of electron (Å)			D (Å)	μ (a.u)
					x	y	z	x	y	z		
S1	0.7691	0.6102	0.0094	0.2541	-7.9403	3.8413	0.3515	-5.6705	2.1743	-0.4398	2.92	3.81
S2	0.7405	0.5902	0.0126	0.2818	6.4142	1.9438	-1.0686	5.3541	0.5802	-1.5402	1.79	2.25
S3	0.8025	0.5856	-0.0019	0.4560	-11.2254	4.5841	0.8403	-11.5454	4.8968	0.9807	0.46	0.61
S4	0.7566	0.5934	-0.0069	0.1904	10.3535	0.2212	0.2506	9.6245	0.8917	-1.6113	2.10	2.69
S5	0.5676	0.4205	0.0004	0.2716	4.4241	-0.5533	-0.3266	3.3030	-0.4533	-0.2063	1.13	1.05
T1	0.5318	0.4116	0.0038	0.2919	7.8741	0.1186	-1.4481	7.5034	0.1056	-1.8300	0.53	0.47
T2	0.4316	0.3399	-0.0077	0.1982	-8.4315	2.6609	0.1632	-7.4473	2.5838	-0.2036	1.05	0.76
T3	0.4098	0.2830	-0.0004	0.2018	10.2128	0.0759	0.4798	8.7160	-0.2149	0.9710	1.60	1.04
T4	0.3266	0.2375	0.0004	0.1844	-0.0502	1.9333	-0.4371	-0.2161	0.8929	-0.3920	1.05	0.56
T5	0.3614	0.2664	-0.0089	0.2244	-1.6445	2.6263	-0.2319	-1.0206	2.6156	-0.3184	0.62	0.37

Table S7. Computed RMSD of electron and hole, H index and t index for singlet states of TPA-2PPITPA.

State	RMSD (Electron)				RMSD (Hole)				H index				t index			
	x	y	z	total	x	y	z	total	x	y	z	Total	x	y	z	Total
S1	4.749	2.069	0.831	5.246	6.073	2.771	0.889	6.735	5.411	2.420	0.860	5.990	-4.949	-2.354	-0.847	5.545
S2	4.360	1.970	0.915	4.871	6.707	2.283	1.024	7.158	5.534	2.126	0.970	6.007	-4.732	-1.275	-0.632	4.942
S3	4.544	2.229	0.829	5.129	4.355	3.091	0.927	5.420	4.450	2.660	0.878	5.258	-2.410	-2.185	-0.818	3.354
S4	4.173	2.316	1.165	4.913	4.743	2.338	1.004	5.383	4.458	2.327	1.084	5.145	-4.267	-2.294	-1.059	4.959
S5	4.569	2.446	0.893	5.259	4.509	2.204	0.862	5.092	4.539	2.325	0.877	5.175	-4.032	-2.069	-0.840	4.609
T1	5.007	2.172	1.045	5.557	5.634	2.431	1.037	6.224	5.320	2.302	1.041	5.890	-4.862	-2.010	-0.916	5.340
T2	5.041	2.421	0.878	5.661	5.409	2.383	0.884	5.976	5.225	2.402	0.881	5.818	-5.191	-2.081	-0.846	5.657
T3	6.065	2.680	1.104	6.722	5.922	2.558	1.166	6.555	5.993	2.619	1.135	6.638	-5.798	-2.528	-1.103	6.420
T4	7.403	3.066	1.128	8.091	6.724	2.902	1.138	7.412	7.063	2.984	1.133	7.751	-5.608	-2.423	-0.952	6.183
T5	6.307	2.857	0.973	6.992	6.667	2.941	1.063	7.364	6.487	2.899	1.018	7.178	-5.308	-1.992	-0.960	5.750

Table S8. Computed RMSD of electron and hole, H index and t index for triplet states of TPA-2SPPITPA

State	RMSD (Electron)				RMSD (Hole)				H index				t index			
	x	y	z	total	x	y	z	total	x	y	z	Total	x	y	z	Total
S1	6.858	2.302	1.165	7.327	8.083	2.741	1.495	8.665	7.471	2.521	1.330	7.996	-5.201	-0.854	-0.539	5.298
S2	7.248	2.378	1.232	7.727	9.184	3.156	1.547	9.833	8.216	2.767	1.389	8.780	-7.156	-1.403	-0.918	7.350
S3	4.366	2.237	1.387	5.098	3.250	2.437	1.333	4.275	3.808	2.337	1.360	4.670	-3.488	-2.024	-1.220	4.213
S4	3.184	1.990	1.400	4.007	3.326	2.712	2.080	4.769	3.255	2.351	1.740	4.376	-2.526	-1.681	0.122	3.037
S5	8.196	2.906	1.761	8.873	8.084	2.943	1.899	8.811	8.140	2.924	1.830	8.841	-7.019	-2.824	-1.709	7.757
T1	4.485	2.113	0.973	5.053	4.667	2.360	1.378	5.408	4.576	2.236	1.176	5.227	-4.205	-2.223	-0.794	4.823
T2	5.419	2.277	1.152	5.990	5.087	3.286	1.328	6.200	5.253	2.781	1.240	6.072	-4.269	-2.704	-0.873	5.128
T3	6.464	2.221	1.617	7.023	3.441	2.487	2.058	4.718	4.952	2.354	1.837	5.783	-3.456	-2.063	-1.346	4.244
T4	9.549	3.932	1.692	10.46	10.60	3.840	1.709	11.40	10.07	3.886	1.700	10.93	-9.911	-2.845	-1.655	10.443
T5	11.03	3.402	1.680	11.66	11.04	3.615	1.712	11.74	11.04	3.509	1.696	11.70	-10.416	-3.498	-1.609	11.105

Table S9. Transferred charges (q_{CT}), barycentres of electron density loss (R_+) /gain (R-), distance between two barycenters (D_{CT}), dipole moment of CT (μ_{CT}), RMSD of +ve/-ve regions, CT indices (H & t) and overlap integral of C+/C- of TPA-2PPITPA and TPA-2SPPITPA.

Emissive materials	**q_{CT}** $\lvert e^{-1} \rvert$	**R_+ (Å)**			**R- (Å)**			**D_{CT} (Å)**	**μ_{CT} (D)**	**RMSD of +ve** regions	**RMSD of -ve** regions	**H /t indices (Å)**	**overlap integral of C+/ C-**
TPA-2PPITPA	32.086 - 32.496	0.383	-0.701	0.134	0.902	-0.593	0.061	0.535	32.460	17.513	17.407	9.239/8.714	0.9969
TPA-2SPPITPA	33.002 - 33.146	-4.323	-0.189	-0.121	-2.378	-0.645	1.094	2.337	33.606	22.036	22.551	11.777/9.613	0.9335

Table S10. Summary of device efficiencies and current state-of-the-art literature data for connection strategy based emitters based OLEDs.

Emitter	V_{on} [V]	CE (cd/A)	EQE (%)	PE (lm/W)	EL (nm)	Ref.
TPA-2SPPITPA	**2.8**	**5.92**	**6.13**	**5.15**	**438**	**This work**
TPA-2PPITPA	**2.9**	**5.43**	**5.82**	**4.98**	**444**	**This work**
m TPE- *m* TPE	3.9	2.1	1.9	1.7	452	10
m TPE- *p* TPE	4.1	2.8	1.9	2.0	459	10
*m*TPE-2*m*TPE	4.7	1.88	1.30	1.36	449	11
*p*TPE-2*m*TPE	3.7	4.03	2.17	2.79	471	11
mTPE-2pTPE	3.5	3.67	2.09	2.90	461	11
Si-*p*-TPE	3.5	7.40	2.92	5.57	512	12
Si-tPE	3.0	8.04	3.38	6.17	488	12
Si-*m*TPE	3.7	1.39	1.21	1.18	432	12
py2	3.4	2.44	-	1.85	460	13
*m*py2	3.6	2.26	-	1.56	438	13
*m*TPA–PPI	3.2	0.84	3.33	0.48	404	7
26BTPIPy	2.8	4.16	5.15	4.35	440	14
25BTPIPy	3.0	6.22	4.72	5.89	460	14
3,3'-BNPIB	3.0	7.12	3.44	6.13	425	15
4,4'-BNPIB	3.1	6.45	3.23	5.42	448	15
m-BBTPI	3.2	1.99	3.63	1.81	428	16
BBTPI	2.7	4.58	5.77	4.77	448	16
L-BPPI	4.5	-	-	0.68	411	8
Z-BPPI	5.0	-	-	0.31	368	8
*m*PA-PTPI	3.8	-	1.85	-	438	17
*m*PA-PPPI	3.0	-	3.90	-	438	17
*m*NA-PTPI	4.2	-	2.80	-	425	17
*m*NA-PPPI	3.0	-	3.49	-	427	17

References

[1] J. Jayabharathi, S. Panimozhi, V. Thanikachalam, *Sci Rep.* 2020, **10**, 5114.

[2] (a) M. J. Frisch, G. W. Trucks, H. B. Schlegel, G. E. Scuseria, M. A. Robb, J. R. Cheeseman, G. Scalmani, V. Barone, B. Mennucci, G. A. Petersson, H. Nakatsuji, M. Caricato, X. Li, H. P. Hratchian, A. F. Izmaylov, J. Bloino, G. Zheng, J. L. Sonnenberg, M. Hada, M. Ehara, K. Toyota, R. Fukuda, J. Hasegawa, M. Ishida, T. Nakajima, Y. Honda, O. Kitao, H. Nakai, T. Vreven, J. A. Montgomery, Jr., J. E. Peralta, F. Ogliaro, M. Bearpark, J. J. Heyd, E. Brothers, K. N. Kudin, V. N. Staroverov, R. Kobayashi, J. Normand, K. Raghavachari, A. Rendell, J. C. Burant, S. S. Iyengar, J. Tomasi, M. Cossi, N. Rega, J. M. Millam, M. Klene, J. E. Knox, J. B. Cross, V. Bakken, C. Adamo, J. Jaramillo, R. Gomperts, R. E. Stratmann, O. Yazyev, A. J. Austin, R. Cammi, C. Pomelli, J. W. Ochterski, R. L. Martin, K. Morokuma, V. G. Zakrzewski, G. A. Voth, P. Salvador, J. J. Dannenberg, S. Dapprich, A. D. Daniels, O. Farkas, J. B. Foresman, J. V. Ortiz, J. Cioslowski and D. J. Fox, Gaussian, Inc., Wallingford CT (Revision A.02), *Gaussian, Inc., Wallingford, CT.* 2009. (b) T. Lu, F. Chen, *J. Comput. Chem.* 2012, **33**, 580.

[3] R. L. Martin, *J. Chem. Phys.* 2003, **118**, 4775.

[4] T. Le Bahers, C. Adamo and I. Ciofini, *J. Chem. Theory Comput.* 2011, **7**, 2498.

[5] S. Tretiak and S. Mukamel*, Chem. Rev.* 2002, **102**, 3171.

[6] J. Jayabharathi, R. Ramya, V. Thanikachalam, P. Jeeva and E. Sarojpurani, *RSC Adv*. 2019, **9**, 2948.

[7] H. Liu, Q. Bai, L. Ya, H. Zhan, H. Xu, S. Zhang, W. Li, Y. Gao, J. Li, P. Lu, H. Wang, B. Yang and Y. Ma, *Chem. Sci.* 2015, **6**, 3797.

[8] Z. Wang, Y. Feng, H. Li, Z. Gao, X. Zhang, P. Lu, P. Chen, Y. Mab and S. Liu, *Phys. Chem. Chem. Phys.* 2014, **16**, 10837.

[9] Y. F. Chang, H. F. Meng, G. L. Fan, K. T. Wong, H. W. Zan, H. W. Lin, H. L. Huang and S. F. Horn, *Org. Electron.* 2016, **29**, 99.

[10] J. Huang, N. Sun, Y. Dong, R. Tang, P. Lu, P. Cai, Q. Li, D. Ma, J. Qin and Z. Li, *Adv. Funct. Mater.* 2013, **23**, 2329.

[11] J. Huang, N. Sun, J. Wang, R. Tang, X. Li, J. Dong, Q. Li, D. Ma and Z. Li, *Isr. J. Chem*. 2014, **54**, 931.

[12] J. Yang, N. Sun, J. Huang, Q. Li, Q. Peng, X. Tang, Y. Dong, D. Ma and Z. Li, *J. Mat. Chem. C.* 2015, **3**, 2624.

[13] R. Zhang, H. Sun, Y. Zhao, X. Tang and Z. Ni, *Dyes and Pigments*, 2018, **152**, 1.

[14] Z. L. Zhu, W. C. Chen, L. D. Zhang, X. L. Liu, Q. X. Tong, F. L. Wong, F. Lua and C. S. Lee, *J. Mater. Chem. C*, 2016, **4**, 1.

[15] J. Jayabharathi, A. Prabhakaran, V. Thanikachalam and P. Jeeva, RSC, *New J. Chem.* 2016, **40**, 8768.

[16] W. C. Chen, G. F. Wu, Y. Yuan, H. X. Wei, F. L. Wong, Q. X. Tong and C. S. Lee, *RSC Adv.*, 2015, **5** 18067.

[17] A. Pachariyangkun, W. Senapak, T. Sudyoadsuk, S. Namuangruk and V. Promarak, 2020, **85**, 105897.